Fabrication of stretchable, flexible conductive thermoplastic polyurethane/graphene composites *via* foaming†

Yuejuan Chen,[a] Yang Li,[a] Donghua Xu*[b] and Wentao Zhai*[a]

Stretchable and flexible conductive polymers have aroused great interest recently because of their applications in the fields of novel electronics, such as smart textiles, artificial electronic skin, flexible electronic displays, *etc.* In this work, stretchable and flexible conductive thermoplastic polyurethane (TPU)/graphene composite foams have been developed by water vapour induced phase separation. The as-prepared TPU/graphene composite foams exhibited a lower modulus, larger elongation at break, and lower hysteresis during a cycle tensile test than a TPU/graphene composite did. It is expected that the improved elasticity of the TPU/graphene composite foams was caused by the deformation of cells, which partially offset the deformation of the TPU matrix. In addition, the cell walls divided the whole composites into many small parts, which could further restrain plastic deformation of hard segment domains under deformation.

1 Introduction

Recently, a class of stretchable electronic materials has aroused extensive interest because of their various applications in hi-tech fields of novel electronics, such as flexible strain sensors for human-motion detection and tactile sensors for electronic skins.[1,2] With stretchable smart sensors, sensitivity is a prerequisite and is very important. In addition, low hysteresis, high repeatability and excellent durability are also crucial to extend their lifetime.[3–5] Moreover, the sensors should be lightweight, and highly stretchable to follow all the mechanical deformations of the textile materials without affecting the original textile characteristics such as softness, feel, *etc.* Among all the materials under research, conductive elastic composites (CECs) are one sort of material which possess these specifications because of their advantages of stretchability, mechanical robustness, light weight and low-cost fabrication.[6,7] There are a variety of approaches to develop CECs, blending conductive fillers with elastic polymers is one of the most attractive methods due to the advantages of process simplicity, cost-effectiveness and tuning of conductivity. However, it is hard to simultaneously acquire high conductivity by increasing the proportion of conductive fillers and keep the outstanding mechanical and elastic properties which originate from the elastic polymer,[8,9] which will eventually affect the repeatability and durability or sensitivity of the stretchable smart sensors. Other methods like filling micro-channels with liquid metals and infiltrating elastomers in conductive-filler networks[10–14] may solve the problem, but will bring other problems like high cost or poor long term stability. Therefore, better solutions are needed to meet the requirements of smart sensors in human-motion detection.

Thermoplastic polyurethane (TPU) elastomers are multi-block copolymers composed of soft and hard segments, which demonstrate thermodynamic incompatibility at room temperature, which consequently, results in microphase separation. The elasticity of TPU, which can be characterized either by stiffness and strain recovery or inversely, by hysteresis and stress relaxation, is a crucial property in commercial competition with other thermoplastic elastomers.[15] In order to obtain more functionality, such as conductivity and high mechanical strength, many researchers prepared TPU based composites by adding functional nanofillers into the TPU matrix.[16–19] However, it is hard to find a win–win solution between acquiring high conductivity or high mechanical strength and achieving high strain at break. For example, Choi *et al.* found that the addition of functionalized graphene endowed TPU with high conductivity and an enhanced modulus, but reduced its tensile strength and elongation at break dramatically.[20]

Foaming is usually considered an effective way to prepare lightweight materials and to reduce cost. There are many methods to introduce cell structures to TPU, such as *in situ* polymerization using water as a foaming agent, batch foaming

[a]*Ningbo Key Lab of Polymer Materials, Ningbo Institute of Material Technology and Engineering, Chinese Academy of Sciences, Ningbo, Zhejiang Province, 315201, China. E-mail: wtzhai@nimte.ac.cn*

[b]*State Key Lab of Polymer Physics and Chemistry, Changchun Institute of Applied Chemistry, Chinese Academy of Sciences, Changchun 130022, China. E-mail: dhxu@ciac.ac.cn*

by CO_2, salt leaching, and phase inversion.[21–29] Among all of these, water vapour induced phase separation (WVIPS) is a facile and low-energy-consuming approach to prepare microcellular nanocomposites with both fine cell structures and a high content of nanofillers.

Graphene, a newly discovered 2D carbon nanomaterial, not only possesses a high Young's modulus but also exhibits a high specific surface area and excellent electronic conductivity. These properties make graphene very promising in fabricating CECs, supercapacitors, thermoelectric materials, *etc.*[30–33] In this article, to prepare a stretchable conductive material, graphene was used to endow TPU with high strength and good electronic conductivity. At the same time, microcellular structures were introduced to the TPU matrix by the WVIPS method to obtain a better elasticity.

2 Experimental

2.1 Materials

TPU (E180) was purchased from Miracll Chemicals Co. (China), and dehydrated at 80 °C for 4 h. Graphene sheets with a specific surface area of 700 $m^2\ g^{-1}$ were prepared using the Staudenmaier method as reported in our previous work.[34] Each graphene platelet was composed of 3–4 individual graphene sheets because the specific surface area is about 3.5 times lower than the ideal specific surface area (2630 $m^2\ g^{-1}$) of a single graphene sheet.[35] *N*,*N*′-Dimethylformamide (DMF) was supplied by Sinopharm Chemical Reagent (China) and used as received.

2.2 Fabrication of TPU/graphene nanocomposites

A typical solution blending method was used to prepare the TPU/graphene nanocomposites (Fig. 1). First, a certain amount of graphene (1.0 g) was dispersed in DMF (100 mL) with the assistance of ultrasonication for 90 min. Second, TPU pellets (20.0 g) were added and stirred overnight at 70 °C. The resultant solution was added dropwise into an excess of deionized water to get a precipitate of TPU/4.8 wt% graphene nanocomposites. After filtration and washing several times with deionized water, the precipitate was dried at 80 °C for 48 h to remove the residual water. Finally, the dried precipitate was disintegrated into powder for further experiments.

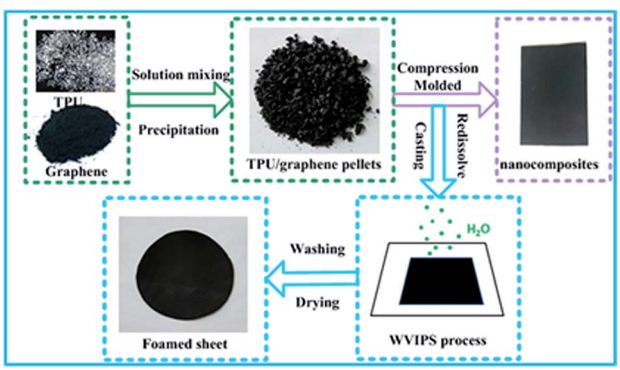

Fig. 1 Diagram for the preparation of the TPUG and TPUGF.

TPU/graphene nanocomposites (TPUG) were prepared by a hot press at 200 °C, and then cooled in air. TPUG with 0, 5, 10, 15 and 20 phr (parts per hundred of resin) graphene were coded as TPUG0, TPUG5, TPUG10, TPUG15 and TPUG20, respectively.

2.3 Preparation of TPU/graphene nanocomposite foams

TPU/graphene composite foams were prepared by WVIPS as described in our previous work.[29] The as-prepared TPU/graphene powders with different concentrations of graphene were dissolved in DMF under mechanical agitation for 24 h at 70 °C to form homogeneous solutions. After being kept under stirring for 30 min, the solutions were cast into films on a flat glass and exposed to the air under a temperature of 20 °C and humidity of 80%. Then the solidified TPU/graphene foam sheets were immersed in cold water to remove the residual DMF and dried at 80 °C for 24 h. A series of TPU/graphene foams (TPUGF) containing 0, 5, 10, 15 and 20 phr graphene were prepared, and were coded as TPUGF0, TPUGF5, TPUGF10, TPUGF15 and TPUGF20, respectively.

2.4 Characterization

The densities of TPUG and TPUGF were measured by the water displacement method according to ASTM D792. The hardness of all samples was measured by a Shore A durometer according to ASTM D2240.

The foam morphology was observed by a Hitachi TM-1000 scanning electron microscope (SEM). The cell structure before and after a cycle test was studied by a Hitachi S-4800 field emission SEM at an accelerating voltage of 4 kV.

The volume electrical conductivity of moderately conductive samples ($>1 \times 10^{-8}$ S cm^{-1}) was measured using a standard four-probe method on a Napson Cresbox Measurement System. The samples with rather low conductivity ($\leq 1 \times 10^{-8}$ S cm^{-1}) were measured with a three-terminal fixture on an EST121 ultrahigh resistance and microcurrent meter (Beijing EST Science & Technology CO. Ltd) in accord with ASTM D257.

The mechanical and elastic properties of the TPUG and TPUGF samples were measured using a universal testing machine, the Instron 5567, while all specimens were 100 mm × 10 mm × 1 mm and at least three specimens were tested for each sample. The elasticity is characterized by the hysteresis of the load–unload curves and residual strain in the cycle tensile test. To compare the hysteresis of different samples, a cycle test at 25 mm min^{-1} was performed and the relative hysteresis of each sample was calculated. The relative hysteresis for a given cycle is calculated by the ratio of the area bounded by the loading–unloading curves to the total area under the loading curve.[36]

3 Results

3.1 Foam structure characterization of TPUG and TPUGF

Table 1 shows the densities and hardness of TPUG and TPUGF. The density of TPUG slightly increases from 1.18 to 1.27 g cm^{-3} with graphene loading increasing from 0 to 20 phr. After the foaming, however, the density of TPUGF is in the range of 0.39–

Table 1 Density and hardness of TPUG and TPUGF samples

Graphene content		Density (g cm^{-3})		Hardness (Shore A)	
(phr)	(wt%)	TPUG	TPUGF	TPUG	TPUGF
0	0	1.18	0.40	78	36
5	4.8	1.24	0.40	>90	44
10	9.1	1.25	0.41	>90	50
15	13.0	1.25	0.39	>90	52
20	16.7	1.27	0.40	>90	55

0.41 g cm^{-3}, showing about a threefold volume expansion. The hardness of TPUG0 is about 78. After the addition of graphene, the hardness of TPUG significantly increases to a value exceeding 90. With the introduction of cell structures, however, the hardness of TPUGF reduces to a range of 36 to 55. It is obvious that foaming is an effective way to prepare lighter and softer TPU composites.

As indicated in Fig. 2a, the foamed TPUG sheets show good flexibility and can be folded and flattened easily under a weak force. Fig. 2b shows the fractured SEM images of TPUGF. It is clear that TPUGF presents a uniform cell structure, and the increase in graphene content tends to decrease the cell size of TPUGF from 12.7 μm for TPUGF0 to 7.6 μm for TPUGF20 (Fig. 2c). This is probably due to the increased viscosity of the solution at high graphene loading, which restrains the cell growth process.[37]

3.2 Mechanical properties of TPUG and TPUGF

The representative stress–strain curves of TPUG and TPUGF under a tensile rate of 500 mm min^{-1} are presented in Fig. 3. TPUG0 exhibits a typical elastomer stress–strain curve, where an approximately linear region at low strain is followed by a plateau region. At a strain of higher than 600%, the stress

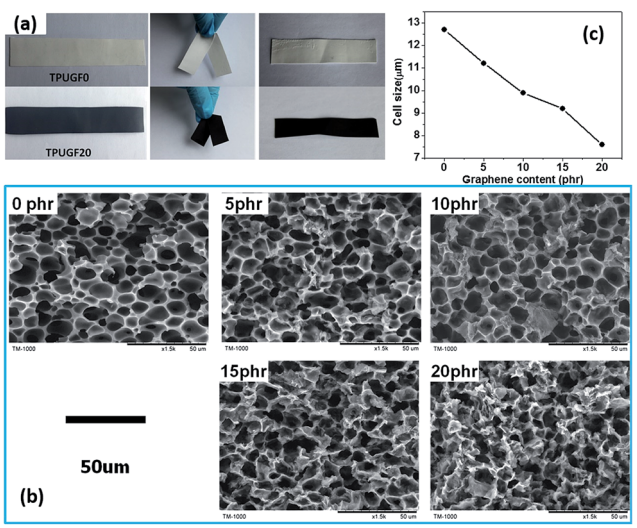

Fig. 2 Optical photographs (a), SEM micrographs (b) and cell size (c) of TPUGF samples as a function of graphene content.

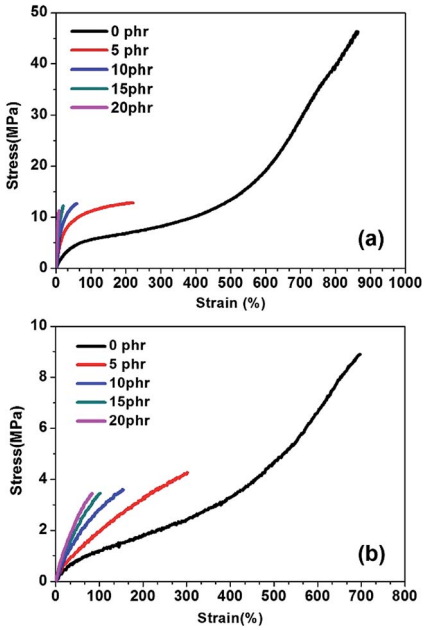

Fig. 3 Stress–strain curves of TPUG (a) and TPUGF (b) as a function of graphene content.

increases due to strain hardening. TPUGF0 presents a similar stress–strain curve to that of TPUG0, characterized by softness and high ductility. The addition of graphene affects the stress–strain curve of TPU significantly, and the as-obtained TPUG with varying graphene loading exhibits a brittle characteristic. In the case of TPUGF, it is still brittle, but its ductility increases obviously relative to its unfoamed counterpart.

Table 2 lists the mechanical properties of TPUG and TPUGF. The increased Young's modulus (E) of TPUG and TPUGF with increased graphene loading is caused by the reinforcing effect of graphene.[31,38] However, the incorporation of graphene significantly reduces the elongation at break of TPU. The reason is due to aggregates of graphene (Fig. S1†) within the TPU matrix, which may act as defects during the tensile testing process and decrease the elongation at break of TPUG.[20,38] With the introduction of cell structures, it is inspiring to find that the elongation at break of TPUGF samples is much higher than the corresponding TPUG samples.

3.3 Elasticity of TPUG and TPUGF

The elasticity of TPUG and TPUGF has been characterized by hysteresis energy loss and residual strain in a cycle tensile test. The typical load–unload curves of TPUG0 and TPUG5 at an increasing strain level are presented in Fig. 4a and b. The hysteresis energy and residual strain at different strain levels have also been calculated and fitted into smooth curves, as presented in Fig. 4c and d. TPUG5 and TPUG10 underwent the cycle test under the same conditions until the samples were broken, TPUG15 and TPUG20 were too brittle to perform the cycle test, so only the data of TPUG0, TPUG5, and TPUG10 are presented here. Firstly, it is obvious that the hysteresis of the TPUG sample is strain dependent, which demonstrates that

Table 2 Mechanical properties of TPUG and TPUGF as a function of graphene content

Graphene content (phr)	Young's modulus (MPa)		Tensile strength (MPa)		Elongation at break (%)	
	TPUG	TPUGF	TPUG	TPUGF	TPUG	TPUGF
0	15.2 ± 2.3	2.7 ± 0.3	46.3 ± 3.4	8.9 ± 1.0	863.3 ± 73.5	696.7 ± 20.4
5	41.7 ± 3.6	3.9 ± 0.2	12.9 ± 1.2	4.5 ± 0.5	220.0 ± 16.2	301.7 ± 35.5
10	62.4 ± 5.8	5.0 ± 0.3	12.7 ± 0.3	3.6 ± 0.4	58.8 ± 5.6	155.0 ± 15.4
15	83.1 ± 2.4	6.8 ± 0.2	12.2 ± 0.6	3.5 ± 0.7	20.0 ± 5.7	101.7 ± 10.1
20	96.9 ± 2.7	7.8 ± 0.6	11.3 ± 0.8	3.3 ± 0.4	8.3 ± 6.2	83.3 ± 7.6

there is more hysteresis generated at a higher strain. Subsequently, compared to TPUG0, the hysteresis of TPUG increases greatly with increasing graphene content. The residual strain shows a similar trend as the hysteresis curves: bigger strain, bigger residual strain; higher graphene content, bigger residual strain. However, the residual strain–strain curves are almost linear, while the curve of hysteresis *versus* strain tends to be stable at a higher strain. This means that the residual strain of the TPUG samples is much more sensitive to strain than their hysteresis.

The typical load–unload curves of TPUGF0 and TPUGF5 at an increasing strain level are shown in Fig. 5a and b. The hysteresis and residual strain at different strain levels were calculated and the results are shown in Fig. 5c and d, respectively. Similar results as in the case of TPUG could be concluded. The hysteresis and residual strain are higher at larger strain or higher graphene content.

The elasticity of TPUG and TPUGF samples has been compared below. Taking the hysteresis data for example, the hysteresis of TPUGF0 is 39.8% at 400%, reduced by 18.0% compared to TPUG0 (47.8%); the hysteresis of TPUGF5 is 44.7% at 75%, reduced by 14.9% compared to TPUG5 (59.6%); for the sample containing 10 phr graphene, the reduction is 13.5% at 50% strain. From the above results, it is observed that the TPUG samples show more hysteresis (more energy loss) than the TPUGF samples at the same strain, and the difference in hysteresis between TPUG and TPUGF becomes larger as the graphene content increases. Namely, the elasticity of TPUG increases with the introduction of a porous structure.

To understand the influence of a foam structure on the elastic behaviour of TPUG and TPUGF samples, further experiments were performed for samples without graphene, below. We conducted a cycle test with five load–unload cycles for typical TPUG0 and TPUGF0 samples at a fixed strain of 43%, using a constant tensile rate of 25 mm min^{-1}. In Fig. 6a and b, both TPUG0 and TPUGF0 show a significant Mullins effect (cyclic softening). The cycle softening, which shows a lower initial modulus in the second and subsequent load–unload cycles, can be explained by breakage and restructuring of hard segment domains.[15] In Fig. 6c, the hysteresis of TPUGF0 is lower

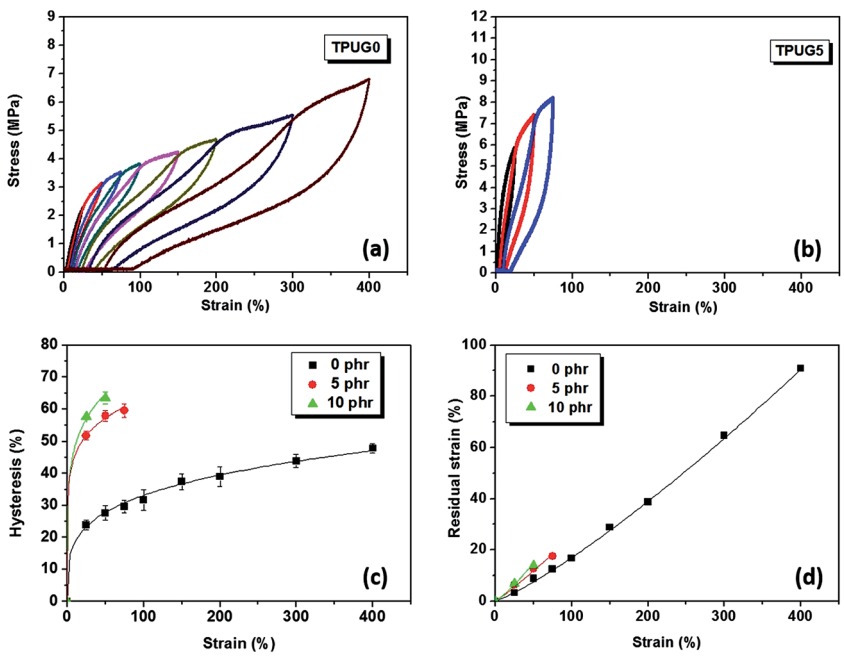

Fig. 4 Elastic properties of TPUG samples. (a) Typical cycle tensile test of TPUG0 with a stepwise increase of strain; (b) typical cycle tensile test of TPUG5 with a stepwise increase of strain; (c) hysteresis energies of TPUG samples *versus* strain; (d) residual strain of TPUG samples *versus* strain.

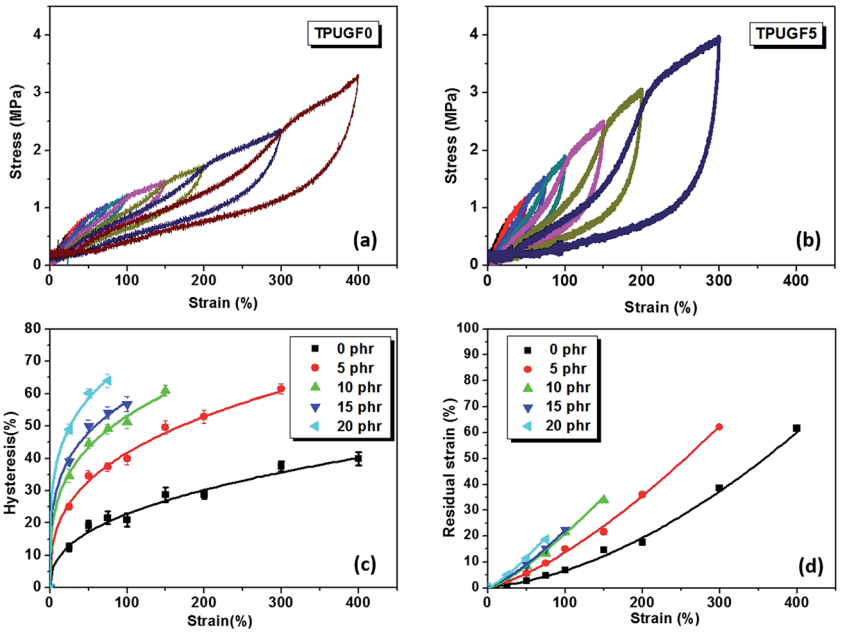

Fig. 5 Elastic properties of TPUGF samples. (a) Typical cycle tensile test of TPUGF0 with a stepwise increase of strain; (b) typical cycle tensile test of TPUGF5 with a stepwise increase of strain; (c) hysteresis energies of TPUGF samples *versus* strain; (d) remaining strain of TPUGF samples *versus* strain.

than TPUG0, which is in accordance with the results presented before. Moreover, the hysteresis decreases as the cycle number increases and then tends to steady at the fifth cycle. This phenomenon has been observed by other researchers and can be explained by the destruction of the weak net-points and orientation of the molecular chains in a more favourable way; eventually an ideal orientated elastic network was formed after two cycles.[39,40] From the results in Fig. 6 for samples without graphene, it is inferred that the foam structure will have the same influence on the elastic behaviour of TPUG and TPUGF samples with graphene.

3.4 Conductivity of TPUG and TPUGF

Generally, the introduction of conductive fillers into insulating polymers will endow the resulting composites with good electrical conductivity.[41,42] As shown in Fig. 7, the direct electrical conductivity for pristine TPU is marginally lower than 1.0×10^{-11} S cm^{-1}, while with the incorporation of only 5 phr graphene, this value increases dramatically to 1.5×10^{-3} S cm^{-1}. The increase is due to the formation of the conductive network in the TPU matrix. Further increasing the graphene loading to 20 phr will lead to a much higher conductivity of 1.3 S cm^{-1}.

In comparison with TPUG, the foamed counterpart, TPUGF, exhibits a much lower electrical conductivity. For example, the electrical conductivity of TPUGF20 is 1.4×10^{-5} S cm^{-1}, lower than the 1.3 S cm^{-1} of TPUG20. The possible reason is that the introduction of cell structures into TPUG compromises the formation of the conductive network to some extent and decreases the paths for charge carrier movement.[18] Nonetheless, the level of electrical conductivity of TPUGF is still sufficient for some applications in semiconductors.[43]

4 Discussion

As the results presented above show, the introduction of cell structures into TPUG composites has improved the strain at break and reduced the hysteresis. Consequently, the as-prepared TPUGF exhibits better mechanical and elastic properties than TPUG. It is rational to ascribe these to the cell structures within TPUGF, which is the biggest difference between them. Fig. 8 presents the cell morphology of TPUGF before and after at least a five cycle tensile test, from which we can see clearly that the cells are elongated and preferentially orientated along the direction of deformation during the test. The elongation of cells can offset some deformation so that the real deformation of TPUGF is less than its TPUG counterpart. As a result, the disruption and plasticity deformation of hard segment domains are restrained, leading to less hysteresis loss for TPUGF.[44] Additionally, the local stress intensification is supposed to be the main reason for the occurrence of the cell coalescence that has been marked by dashed lines in Fig. 8.

In Fig. 9, a schematic picture has been provided to illustrate the structural evolution of TPUGF during the cycle test process. The structure of TPUGF before the tensile test has been sketched in Fig. 9A, in which open cells without deformation are located in the TPUGF matrix.[45] When the sample is under low strain, the cells will be stretched along the extension direction and the cell wall will become much thinner (Fig. 9B). On further increasing the strain over the permanent strain, some cells will reach to their limit, causing the occurrence of cell coalescence (Fig. 9C). In this process, some crystallites in the hard segment domains are partially destroyed and new crystallites are developed simultaneously.[46] After the release of

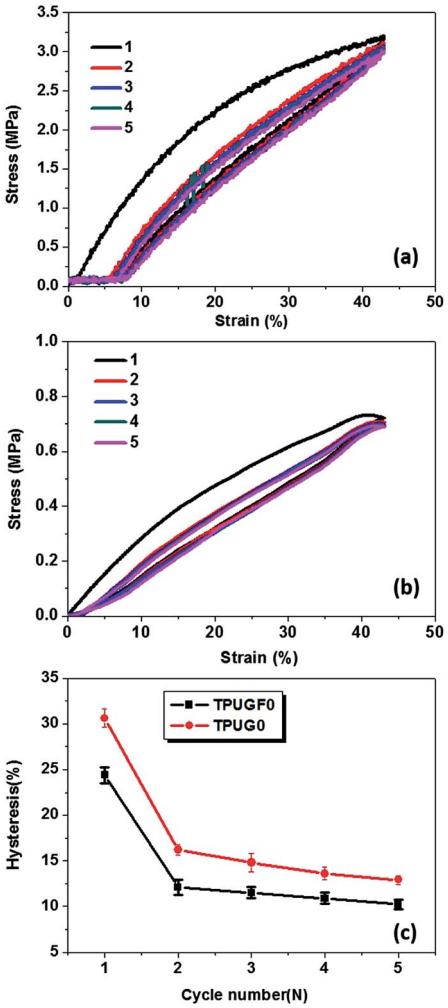

Fig. 6 Cycle tensile test of TPUG0 (a) and TPUGF0 (b) at a fixed strain of 43% with a tensile rate of 25 mm min^{-1}. The hysteresis of each cycle for TPUG0 and TPUGF (c) is obtained from the results in (a) and (b).

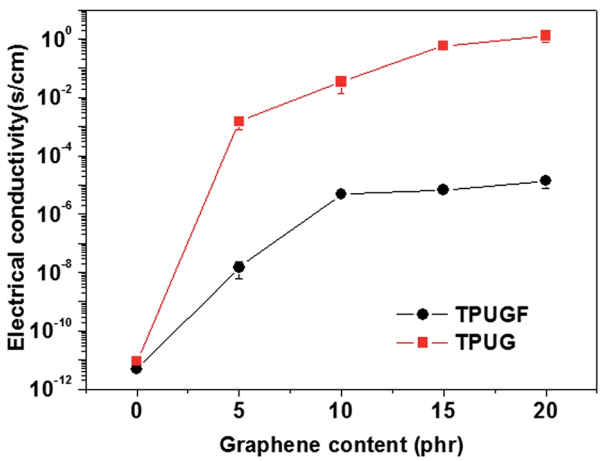

Fig. 7 Electrical conductivity of TPUG and TPUGF.

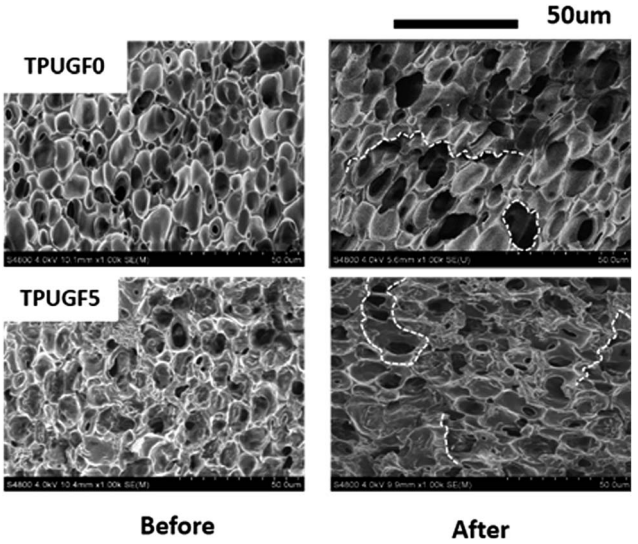

Fig. 8 SEM micrographs of TPUGF samples comparing the differences in cells before and after at least a five cycle test (the dashed lines show typical cell coalescence and cell rupture).

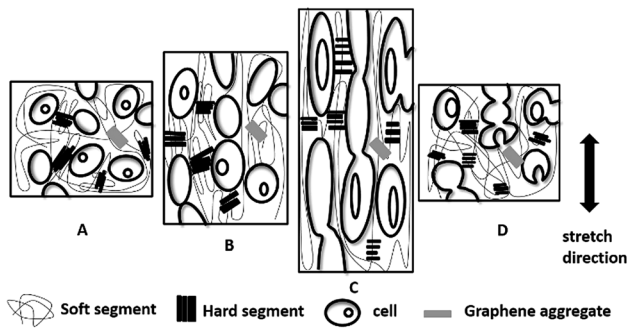

Fig. 9 Schematic picture to illustrate the deformation of cells and hard segments during extension and retraction in the first cycle: (A) before deformation, (B) during extension below the permanent set strain, (C) during extension at a strain larger than the permanent set strain, and (D) during retraction to zero stress. The proportions between the cells, cell walls, hard segment domains and graphene aggregates are not to scale. Not all the cells, hard segments and graphene aggregates are presented.

the stress loaded on TPUGF (Fig. 9D), the cells can recover almost to their original shape except for some cell coalescence as observed in Fig. 8.

The addition of conductive fillers usually makes polymer composites brittle, and have a high modulus, a high hysteresis, and low repeatability. In the present work, however, stretchable and flexible conductive TPUGF has been fabricated and the relationship between cell structure and elasticity was studied based on TPUGF with an open cell structure. The main contribution of this study is that the introduction of a bubble structure makes material soft and can improve the stretching ability of material. Study of the influence on the elasticity of different kinds of cell structures like closed cells or open cells with different porosities is needed in forthcoming work.

5 Conclusions

In summary, we have prepared stretchable conductive TPU/graphene nanocomposite foams through a facile WVIPS method. Compared with their TPUG counterparts, the TPUGF samples have higher elongation at break and better elasticity because of the existence of microcellular structures. Firstly, the deformation of cells can offset partial deformation of the TPU matrix. Secondly, the cell walls can act as a physical barrier to the destruction of hard segments and restrain further plastic deformation of hard segment domains under deformation. The lightweight, conductive, highly stretchable nanocomposite foams present a new possibility for applications in the field of novel electronics.

Acknowledgements

Financial support was provided by National High Technology Research and Development Program of China (863 Program, Grant No. 2013AA032003), National Natural Science Foundation of China (Grant No. 51473181 and 51573202) and China Postdoctoral Science Foundation (Grant No. 2015M570531).

Notes and references

1 T. Yamada, Y. Hayamizu, Y. Yamamoto, Y. Yomogida, A. Izadi-Najafabadi, D. N. Futaba and K. Hata, *Nat. Nanotechnol.*, 2011, **6**, 296–301.
2 T. Sekitani, Y. Noguchi, K. Hata, T. Fukushima, T. Aida and T. Someya, *Science*, 2008, **321**, 1468–1472.
3 Y. Hou, D. R. Wang, X. M. Zhang, H. Zhao, J. W. Zha and Z. M. Dang, *J. Mater. Chem. C*, 2013, **1**, 515–521.
4 H. B. Yao, J. Ge, C. F. Wang, X. Wang, W. Hu, Z. J. Zheng, Y. Ni and S. H. Yu, *Adv. Mater.*, 2013, **25**, 6692–6698.
5 R. Zhang, H. Deng, R. Valenca, J. H. Jin, Q. Fu, E. Bilotti and T. Peijs, *Compos. Sci. Technol.*, 2013, **74**, 1–5.
6 J. H. Kong, N. S. Jang, S. H. Kim and J. M. Kim, *Carbon*, 2014, **77**, 199–207.
7 C. Cochrane, V. Koncar, M. Lewandowski and C. Dufour, *Sensors*, 2007, **7**, 473–492.
8 I. Krupa and I. Chodak, *Eur. Polym. J.*, 2001, **37**, 2159–2168.
9 I. Novak, I. Krupa and I. Chodak, *Synth. Met.*, 2002, **131**, 93–98.
10 M. Kubo, X. F. Li, C. Kim, M. Hashimoto, B. J. Wiley, D. Ham and G. M. Whitesides, *Adv. Mater.*, 2010, **22**, 2749–2752.
11 A. C. Siegel, D. A. Bruzewicz, D. B. Weibel and G. M. Whitesides, *Adv. Mater.*, 2007, **19**, 727–733.
12 M. Park, Y. Xia and U. Jeong, *Angew. Chem.*, 2011, **50**, 10977–10980.
13 F. Xu and Y. Zhu, *Adv. Mater.*, 2012, **24**, 5117–5122.
14 M. Park, J. Park and U. Jeong, *Nano Today*, 2014, **9**, 244–260.
15 C. P. Buckley, C. Prisacariu and C. Martin, *Polymer*, 2010, **51**, 3213–3224.
16 Z. X. Chen and H. B. Lu, *J. Mater. Chem.*, 2012, **22**, 12479–12490.
17 U. Khan, P. May, A. O'Neill, J. J. Vilatela, A. H. Windle and J. N. Coleman, *Small*, 2011, **7**, 1579–1586.
18 E. Bilotti, R. Zhang, H. Deng, M. Baxendale and T. Peijs, *J. Mater. Chem.*, 2010, **20**, 9449–9455.
19 L. Lin, S. Liu, Q. Zhang, X. Y. Li, M. Z. Ji, H. Deng and Q. Fu, *ACS Appl. Mater. Interfaces*, 2013, **5**, 5815–5824.
20 J. T. Choi, D. H. Kim, K. S. Ryu, H. I. Lee, H. M. Jeong, C. M. Shin, J. H. Kim and B. K. Kim, *Macromol. Res.*, 2011, **19**, 809–814.
21 V. Dolomanova, J. C. M. Rauhe, L. R. Jensen, R. Pyrz and A. B. Timmons, *J. Cell. Plast.*, 2011, **47**, 81–93.
22 R. Rizvi and H. Naguib, *J. Mater. Res.*, 2013, **28**, 2415–2425.
23 J. D. Fromstein and K. A. Woodhouse, *J. Biomater. Sci., Polym. Ed.*, 2002, **13**, 391–406.
24 M. T. Khorasani and S. Shorgashti, *J. Biomed. Mater. Res., Part B*, 2006, **76**, 41–48.
25 J. J. Guan, K. L. Fujimoto, M. S. Sacks and W. R. Wagner, *Biomaterials*, 2005, **26**, 3961–3971.
26 Y. Li, X. L. Pei, B. Shen, W. T. Zhai, L. H. Zhang and W. G. Zheng, *RSC Adv.*, 2015, **5**, 24342–24351.
27 B. Shen, W. T. Zhai, M. M. Tao, J. Q. Ling and W. G. Zheng, *ACS Appl. Mater. Interfaces*, 2013, **5**, 11383–11391.
28 W. T. Zhai, Y. J. Chen, J. Q. Ling, B. Y. Wen and Y. W. Kim, *J. Cell. Plast.*, 2014, **50**, 537–550.
29 J. Q. Ling, W. T. Zhai, W. W. Feng, B. Shen, J. F. Zhang and W. G. Zheng, *ACS Appl. Mater. Interfaces*, 2013, **5**, 2677–2684.
30 C. Lee, X. D. Wei, J. W. Kysar and J. Hone, *Science*, 2008, **321**, 385–388.
31 S. Stankovich, D. A. Dikin, G. H. B. Dommett, K. M. Kohlhaas, E. J. Zimney, E. A. Stach, R. D. Piner, S. T. Nguyen and R. S. Ruoff, *Nature*, 2006, **442**, 282–286.
32 M. Moussa, M. F. El-Kady, H. Wang, A. Michimore, Q. Q. Zhou, J. Xu, P. Majeswki and J. Ma, *Nanotechnology*, 2015, **26**, 075702.
33 K. L. Xu, G. M. Chen and D. Qiu, *J. Mater. Chem. A*, 2013, **1**, 12395–12399.
34 H. B. Zhang, Q. Yan, W. G. Zheng, Z. X. He and Z. Z. Yu, *ACS Appl. Mater. Interfaces*, 2011, **3**, 918–924.
35 F. Yavari, M. A. Rafiee, J. Rafiee, Z. Z. Yu and N. Koratkar, *ACS Appl. Mater. Interfaces*, 2010, **2**, 2738–2743.
36 J. A. Miller, S. B. Lin, K. K. S. Hwang, K. S. Wu, P. E. Gibson and S. L. Cooper, *Macromolecules*, 1985, **18**, 32–44.
37 H. C. Park, Y. P. Kim, H. Y. Kim and Y. S. Kang, *J. Membr. Sci.*, 1999, **156**, 169–178.
38 U. Khan, P. May, A. O'Neill and J. N. Coleman, *Carbon*, 2010, **48**, 4035–4041.
39 C. R. Desper, N. S. Schneider, J. P. Jasinski and J. S. Lin, *Macromolecules*, 1985, **18**, 2755–2761.
40 P. Ping, W. S. Wang, X. S. Chen and X. B. Jing, *J. Polym. Sci., Part B: Polym. Phys.*, 2007, **45**, 557–570.
41 A. Ameli, M. Nofar, S. Wang and C. B. Park, *ACS Appl. Mater. Interfaces*, 2014, **6**, 11091–11100.
42 A. Ameli, P. U. Jung and C. B. Park, *Carbon*, 2013, **60**, 379–391.
43 O. T. Ikkala, J. Laakso and K. Vakiparta, *Synth. Met.*, 1995, **69**, 97–100.
44 R. M. Versteegen, R. Kleppinger and R. P. Sijbesma, *Macromolecules*, 2006, **39**, 772–783.

45 Q. Ye, Y. L. Xiang, F. X. Chen, W. L. Xu and H. J. Yang, *Mater. Lett.*, 2013, **100**, 23–25.

46 S. Toki, I. Sics, C. Burger, D. F. Fang, L. Z. Liu, B. S. Hsiao, S. Datta and A. H. Tsou, *Macromolecules*, 2006, **39**, 3588–3597.